ACS APPLIED MATERIALS & INTERFACES

Research Article

Cite This: ACS Appl. Mater. Interfaces 2019, 11, 37885−37891

www.acsami.org

# Targeted Surface Doping with Reversible Local Environment Improves Oxygen Stability at the Electrochemical Interfaces of Nickel-Rich Cathode Materials

James D. Steiner,[†] Hao Cheng,[‡,§] Julia Walsh,[†] Yan Zhang,[∥] Benjamin Zydlewski,[†] Linqin Mu,[†] Zhengrui Xu,[†] Muhammad Mominur Rahman,[†] Huabin Sun,[⊥] F. Marc Michel,[#] Cheng-Jun Sun,[■] Dennis Nordlund,[∥] Wei Luo,[⊥] Jin-Cheng Zheng,[‡,§] Huolin L. Xin,[●] and Feng Lin*[,†]

[†]Department of Chemistry, Virginia Tech, Blacksburg, Virginia 24061, United States

[‡]Department of Physics and the Collaborative Innovation Center for Optoelectronic Semiconductors and Efficient Devices, Xiamen University, Xiamen 361005, China

[§]Xiamen University Malaysia, Sepang, Selangor 439000, Malaysia

[∥]Stanford Synchrotron Radiation Lightsource, SLAC National Accelerator Laboratory, Menlo Park, California 94025, United States

[⊥]Institute of New Energy for Vehicles, School of Materials Science and Engineering, Tongji University, Shanghai 201804, China

[#]Department of Geosciences, Virginia Tech, Blacksburg, Virginia 24061, United States

[■]Advanced Photon Source, Argonne National Laboratory, Argonne, Illinois 60439, United States

[●]Department of Physics and Astronomy, University of California, Irvine, California 92697, United States

Supporting Information

**ABSTRACT:** Elemental doping represents a prominent strategy to improve interfacial chemistry in battery materials. Manipulating the dopant spatial distribution and understanding the dynamic evolution of the dopants at the atomic scale can inform better design of the doping chemistry for batteries. In this work, we create a targeted hierarchical distribution of $Ti^{4+}$, a popular doping element for oxide cathode materials, in $LiNi_{0.8}Mn_{0.1}Co_{0.1}O_2$ primary particles. We apply multiscale synchrotron/electron spectroscopy and imaging techniques as well as theoretical calculations to investigate the dynamic evolution of the doping chemical environment. The $Ti^{4+}$ dopant is fully incorporated into the $TMO_6$ octahedral coordination and is targeted to be enriched at the surface. $Ti^{4+}$ in the $TMO_6$ octahedral coordination increases the TM−O bond length and reduces the covalency between (Ni, Mn, Co) and O. The excellent reversibility of $Ti^{4+}$ chemical environment gives rise to superior oxygen reversibility at the cathode−electrolyte interphase and in the bulk particles, leading to improved stability in capacity, energy, and voltage. Our work directly probes the chemical environment of doping elements and helps rationalize the doping strategy for high-voltage layered cathodes.

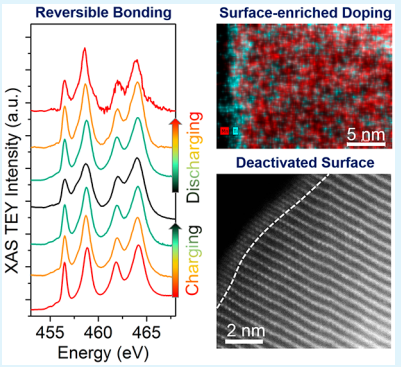


**KEYWORDS:** *battery, cathode, surface doping, oxygen activity, surface chemistry*

Downloaded via XIAMEN UNIV on February 20, 2020 at 07:50:41 (UTC).
See https://pubs.acs.org/sharingguidelines for options on how to legitimately share published articles.

## 1. INTRODUCTION

The large and growing lithium-ion battery market provides strong incentives to continue research, especially as new opportunities in vehicular applications emerge.[1,2] Improving energy density has been a focus of current research in lithium-ion batteries, which can be achieved by elevating the cell operating voltage.[3,4] However, most cathode materials and electrolytic solution undergo severe interfacial reactions at high voltages.[5−7] These interfacial reactions can completely transform the electrochemical interface of cathode particles through surface reconstruction and metal migration, leading to notable capacity fading and impedance buildup.[8−10] Ni-rich layered oxides ($LiNi_{1-x-y}Mn_xCo_yO_2$, NMC) represent a frontier in lithium battery research because of their high energy density and potentially low cost.[11−14] However, the inferior surface and bulk structural stability has become the major roadblock toward the practical implementation of Ni-rich layered oxides ($1 - x - y > 0.75$).[15] The bulk structural instability involves multiple phase transformations, especially the H2−H3 transformation that results in the large charge−discharge hysteresis at high voltages.[16] The surface structural instability is associated with the strong orbital hybridization (covalency) between transition metal (TM) 3d orbitals and oxygen (O) 2p orbitals.[5,17] A high degree of lithium deintercalation increases the TM(3d)−O(2p) hybridization and disrupts the integrity of the layered structure, leading to surface phase transforma-

Received: August 16, 2019
Accepted: September 25, 2019
Published: October 7, 2019


© 2019 American Chemical Society

DOI: 10.1021/acsami.9b14729
ACS Appl. Mater. Interfaces 2019, 11, 37885−37891

tions.[7,18−20] Surface phase transformations usually lead to the release of surface lattice oxygen that participates in the electrolyte oxidation at high voltages.[21] Therefore, limiting oxygen activation has been a long-sought goal for improving the cycle life and energy density of Ni-rich layered oxide cathodes.

Surface coating and bulk elemental doping are among the most popular methods to improve the structural stability at the surface and in the bulk, respectively.[22−24] The technical hurdles are to achieve atomically thin and conformal coating layers on primary particles and to obtain controlled distribution of doping elements in primary particles. Atomic layer deposition (ALD) has been shown to be effective at creating conformal coating layers on NMC secondary particles.[25−27] However, the large-scale manufacturability of the ALD technique remains a major concern for batteries, albeit intensive efforts to commercialize the technique. Doping elements usually have limited solubility in the NMC lattice.[28,29] Upon thermal annealing, the oversaturated doping elements can potentially segregate to the particle surface and form a conformal coating layer.[29] Hypothetically, such process can potentially lead to an optimal doping concentration in the bulk and a conformal coating layer on the surface.[22] Ultimately, this strategy is expected to simultaneously stabilize the surface and bulk structures of NMC particles. Mechanistically, there are some long-standing questions regarding the exact role of elemental doping in stabilizing local chemical environments as well as the dynamic evolution of doping elements upon electrochemical cycling.

Herein, we used $Ti^{4+}$ doping in $LiNi_{0.8}Mn_{0.1}Co_{0.1}O_2$ (NMC811) particles as a model system to manipulate the spatial distribution of the doping element and monitor the evolution of the $Ti^{4+}$ chemical environment at the atomic scale. We synthesized the $Ti^{4+}$-doped NMC811 using a modified coprecipitation method followed by thermal annealing (see Experimental Method). We then performed an in-depth spectroscopic and theoretical investigation on 3%$Ti^{4+}$-doped NMC811 particles (i.e., (Ni + Co + Mn)/Ti = 1/0.03, NMC811-Ti) undergoing extensive electrochemical cycling. The work focuses on investigating the roles of $Ti^{4+}$ surface doping, and the evolution of the dopant chemical environment during electrochemical cycling.

## 2. RESULTS AND DISCUSSION

The pristine NMC811-Ti material had a $R\bar{3}m$ layered structure and a similar X-ray diffraction (XRD) pattern to the baseline NMC811 (Figure S1a, Supporting Information). The $I_{003}/I_{104}$ ratio increased from 1.35 in NMC811 to 1.74 in NMC811-Ti, qualitatively implying that the $Ti^{4+}$ doping limited the initial Li/TM cation mixing.[30] Subsequently, we performed scanning transmission electron microscopy-electron energy loss spectroscopy (STEM-EELS) analysis to probe the $Ti^{4+}$ distribution as well as the surface electronic properties of NMC811-Ti. The particles had a layered structure in the bulk with a slight surface reconstruction layer that was expected in nickel-rich cathode materials (Figure 1a). Furthermore, the high-resolution Ti L-edge XAS demonstrated that $Ti^{4+}$ was fully incorporated in the NMC811 lattice, free of any $TiO_2$ phases (Figure S1b).[31] The EELS scanning shows that $Ti^{4+}$ was present throughout the primary particle and enriched at the top 1−2 nm surface (Figures 1b,c), that is, hierarchical surface doping. We also found that the surface was populated with all four transition metals and that $Ti^{4+}$ might have partially replaced the $Mn^{4+}$

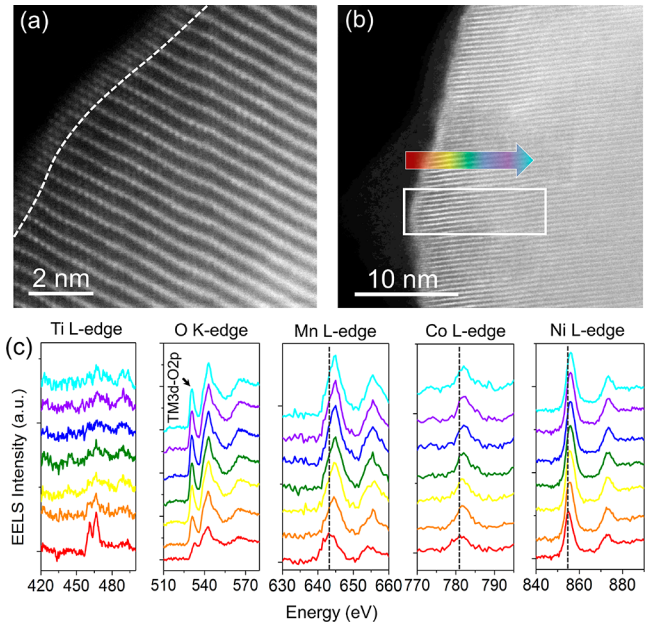


**Figure 1.** Characterization of pristine NMC811-Ti materials. (a) STEM image of the pristine NMC811-Ti particle, where the dashed line separates the surface reconstruction layer from the bulk layered structure. (b) Area of the particle that was analyzed by the EELS scanning. (c) EELS spectra of the transition-metal L-edges and the oxygen K-edge, with the TM(3d)−O(2p) hybridization labeled. Ti was enriched at the top surface. The vertical dashed lines indicate the shift of the edge energy showing that transition metals at the surface are reduced compared to those in the bulk. In (c), the EELS spectra probed deeper from the bottom to the top, as indicated by the arrow in (b).

based on the Ti L-edge and Mn L-edge EELS intensity changes. Meanwhile, the (Ni, Mn, Co) L-edge and O K-edge spectra showed that the surface was slightly reduced. The surface reduction is attributable to the surface reconstruction and the necessity of charge compensation caused by the tetravalent $Ti^{4+}$. Such a reduced surface may potentially inhibit the electrolyte oxidation at the cathode surface during cycling.[32] We found that the doping behavior reported here is different from the $Ti^{4+}$ addition in $LiCoO_2$ materials,[33] likely because of the fact that the NMC lattice is more accommodative for the tetravalent Ti doping.

Our next task is to investigate the battery performance of these materials and to evaluate the suitability of the NMC811-Ti material as the platform to investigate the roles of $Ti^{4+}$ surface doping, and its evolution during electrochemical cycling. Compared to the baseline NMC811, the NMC811-Ti material exhibited improved cycling stability in energy density, discharge capacity, and voltage, which is attributable to the mitigated cell polarization in the NMC811-Ti (Figures 2a,b). When cycled at 1C between 2.5 and 4.5 V vs $Li^+/Li$, the $Ti^{4+}$ doping increased the capacity retention from 69% to 80% over 300 cycles, and from 58% to 70% over 500 cycles (Figure 2c). Such good capacity retentions have been rarely reported for Ni-rich layered oxides such as NMC811 cycled to high voltages (e.g., 4.5 V vs $Li^+/Li$) for 500 cycles.[7,12,34−38] The rate of voltage drop decreased from 0.35 to 0.22 mV/cycle after the $Ti^{4+}$ doping (Figure 2d). The $Ti^{4+}$ doping also increased the energy retention from 54% to 67% over 500 cycles (Figure 2e). The rate capability did not seem to be altered much by the $Ti^{4+}$ doping (Figure S2). Finally, the battery performance of


DOI: 10.1021/acsami.9b14729
ACS Appl. Mater. Interfaces 2019, 11, 37885−37891

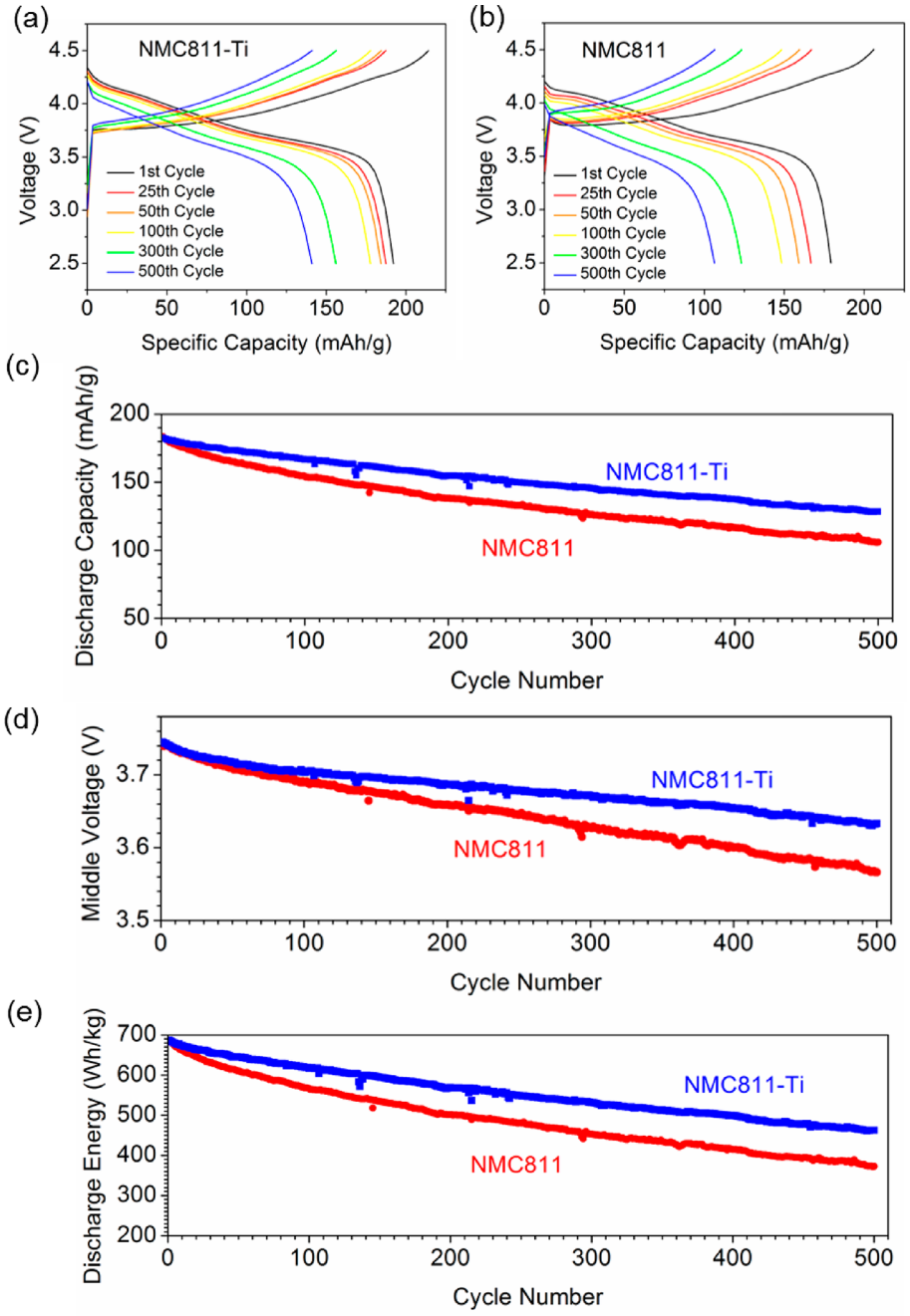


**Figure 2.** Electrochemical performance of cells containing pristine NMC811 and NMC811-Ti materials. (a) Charge−discharge profiles of NMC811-Ti. (b) Charge−discharge profiles of NMC811. (c) Specific discharge capacity as a function of cycle number. The $Ti^{4+}$ doping increased the capacity retention from 69% to 80% over 300 cycles and from 58% to 70% over 500 cycles. (d) Middle voltage (the voltage at 50% discharge capacity) as a function of cycle number. (e) Specific discharge energy as a function of cycle number. The cells were all cycled at 1C between 2.5 and 4.5 V vs $Li^+/Li$ for 500 cycles.

the NMC811-Ti was superior to those of $Ti^{4+}$-doped NMC811 materials synthesized with different $Ti^{4+}$ concentrations or using different methods (Figure S3). Therefore, the performance measurement suggests that the NMC811-Ti can provide a good platform to investigate the roles of $Ti^{4+}$ surface doping, and its evolution during electrochemical cycling.

Probing the evolution of the $Ti^{4+}$ chemical environment and how it stabilizes the electrochemical interface can provide insights into the chemical origin of the improved battery performance. We applied soft XAS Ti L-edge to monitor the reversibility of the $Ti^{4+}$ local chemical environment (Figure 3a). Ti $L_3$-$e_g$ (second peak) and $L_2$-$e_g$ (fourth peak) peaks gradually broadened upon charging and reversibly sharpened upon discharging (Figures 3a and Figure S4). The finite difference method near-edge structure (FDMNES) calculation showed that the broadening was attributed to the reduced Ti−O bond length (Figure S5). The $Ti^{4+}$ local environment was fully reversible after multiple cycles (Figure S6). STEM-EDS mapping of the NMC811-Ti showed that the hierarchical $Ti^{4+}$ distribution remained intact after prolonged cycles (Figure 3b). Ti was still enriched at the surface (~6 at. %) after 300 cycles at 1C between 2.5 and 4.5 V vs $Li^+/Li$. Therefore, one


DOI: 10.1021/acsami.9b14729
ACS Appl. Mater. Interfaces 2019, 11, 37885−37891

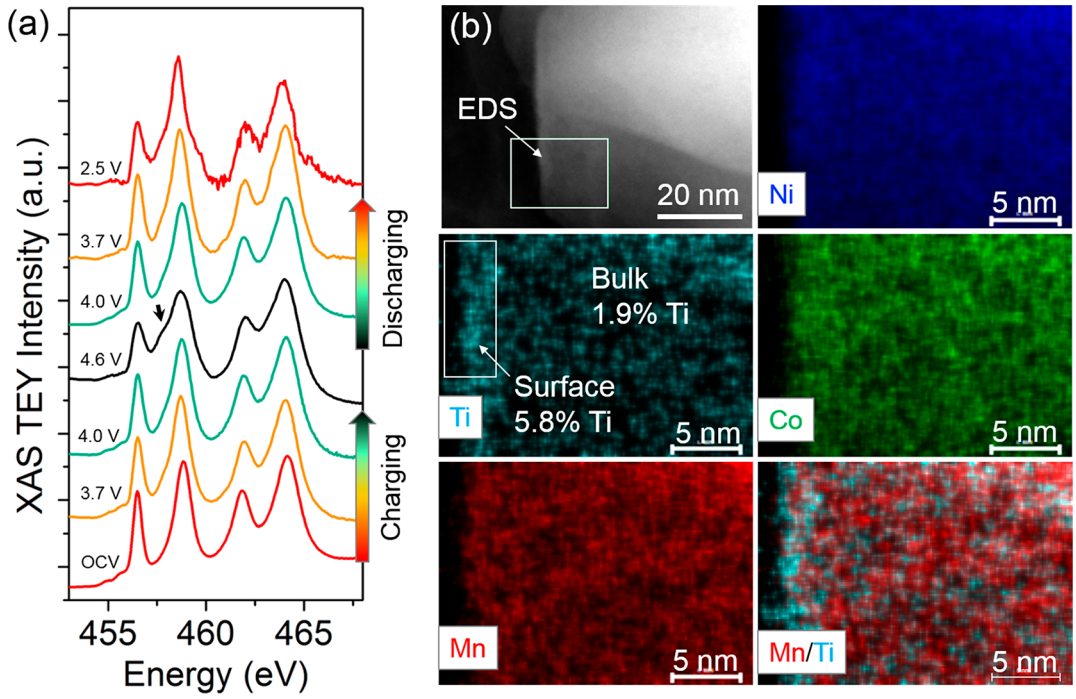


**Figure 3.** Stability of the $Ti^{4+}$ chemical environment. (a) Ti L-edge soft XAS spectra as a function of the state of charge, where the arrow indicates the broadening of the $L_3$-$e_g$ peak (second peak). (b) STEM-EDS mapping of the NMC811-Ti material after 300 cycles at 1C between 2.5 and 4.5 V versus $Li^+/Li$.

can conclude that the $Ti^{4+}$ chemical environment was highly reversible and might be capable of accommodating the strain by changing the Ti−O bond length.

Subsequently, we analyzed the evolution of surface chemistry as a function of the state of charge and cycle number. We expected that surface $Ti^{4+}$ enrichment could decrease the transition-metal−oxygen covalency, thus improving the oxygen stability at the surface.[39] The surface chemistry of layered oxide cathode materials is dominated by the surface reconstruction (i.e., transition-metal reduction, oxygen loss). For Ni-rich layered oxides, nickel cations play the dominant role in the surface reconstruction. Mn and Co cations exhibited relatively high reversibility at the surface of NMC811-Ti (Figure S7). The resilience against surface reconstruction can be characterized by the reversibility of TM(3d)−O(2p) hybridization and quantified by the pre-edge intensity of the O K-edge soft XAS in the TEY mode (Figure S8a). The quantification of the TM(3d)−O(2p) hybridization clearly showed that the NMC811-Ti had deactivated oxygen sites and improved reversibility relative to NMC811 (Figure 4a). In addition, the subsurface oxygen environment, probed by the fluorescence yield (FY) mode, was also highly reversible in the NMC811-Ti material (Figure S9). We further compared the reversibility of surface nickel cations. In general, the Ni oxidation state in NMC811-Ti was more reversible than that in the NMC811 (Figure 4b and Figure S8b). The subsurface nickel oxidation state was reversible in both NMC811-Ti and NMC811(Figure S10). Therefore, our spectroscopic study concluded that the $Ti^{4+}$ doping can stabilize the TM(3d)−O(2p) chemical environment at the surface.

Finally, we studied the impact of $Ti^{4+}$ doping on the bulk chemical environment using hard XAS. The $Ti^{4+}$ doping slightly increased the Ni−O bond length, indicating the decreased Ni−O covalency (Figure S11a). Importantly, such a desirable impact of $Ti^{4+}$ doping remained effective even after

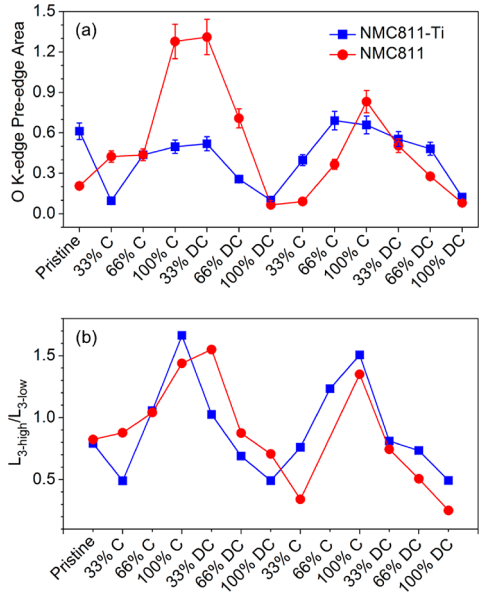


**Figure 4.** Stability of the surface chemistry quantified by soft XAS in the total electron yield (TEY) mode. (a) Integrated area for the TM(3d)−O(2p) hybridization as a function of the state of charge for two cycles. (b) Ni $L_{3\text{-high}}$/Ni $L_{3\text{-low}}$ ratio as a function of the state of charge for two cycles. The cells were cycled at C/10 between 2.5 and 4.6 V vs $Li^+/Li$. The "C" and "DC" represent "charged" and "discharged", respectively.

300 cycles (Figure S11b). It is important to note that the doping effect mainly remained at the surface and the shift is expected to be minor in the EXAFS. The bulk nickel oxidation state remained unchanged after 300 cycles in both NMC811 and NMC811-Ti (Figure S12). Meanwhile, there was no difference in the bulk nickel oxidation state between NMC811



DOI: 10.1021/acsami.9b14729
ACS Appl. Mater. Interfaces 2019, 11, 37885−37891

and NMC811-Ti in the pristine state and after 300 cycles (Figure S13). Furthermore, the changes in (Mn, Co) K-edge XAS were similar in NMC811 and NMC811-Ti (Figure S14). Therefore, the bulk characterization demonstrated that in the bulk the $Ti^{4+}$ doping modified the local bond length and did not alter TM oxidation states. It should be noted that the stability of the NMC811-Ti could be further enhanced if methods were taken to mitigate other fading mechanisms, such as chemomechanical breakdown.

## 3. CONCLUSION

In summary, we developed a hierarchical surface $Ti^{4+}$ doping for Ni-rich layered oxides, at the primary particle level, to stabilize the electrochemical interface undergoing prolonged cycling to high voltages. The hierarchical $Ti^{4+}$ distribution enhanced the reversibility of the TM(3d)−O(2p) hybridization at the surface as well as reducing the TM−O covalency in the bulk. The hierarchical doping was highly stable and remained effective after extensive high-voltage cycling. The resulting NMC811-Ti material exhibited improved stability in energy density, discharge capacity, and voltage. The present study provided mechanistic insights into the chemical and structural origins of the improved stability by surface elemental doping.

## 4. EXPERIMENTAL PROCEDURES

**Materials, Methods, and Characterization.** Synthesis of NMC811-Ti: The materials were synthesized using a modified coprecipitation method ("gradient substitution"). A transition-metal solution of 0.8 M $NiSO_4{\cdot}6H_2O$ (Sigma-Aldrich, 99.99%), 0.1 M $MnSO_4{\bullet}H_2O$ (Sigma-Aldrich, 99%), and 0.1 M $CoSO_4{\cdot}7H_2O$ (Sigma-Aldrich, 99%) was dissolved in 100 mL of aqueous solution with a total metal concentration of 1 M. A base solution of 2 M NaOH and 1.67 M $NH_3{\cdot}H_2O$ was diluted to 100 mL of aqueous solution. Each solution was stored in a Kimble bottle and the base solution was under the $N_2$ protection. A titanium solution was made using a titanium oxysulfate solution (Sigma-Aldrich, 15 wt % in dilute sulfuric acid). Titanium oxysulfate (0.003 mol) was diluted to a 50 mL aqueous solution. This titanium solution was stored in its own Kimble bottle. 1 M NaOH and 0.83 M $NH_3{\cdot}H_2O$ were diluted to 160 mL in deionized (DI) water and then placed into the reaction vessel. The vessel was heated to 50 °C, protected with $N_2$ gas, and stirred continuously starting at 600 rpm. The pH was adjusted to ∼10.5. The transition-metal solution and base solution were pumped into the reaction vessel at approximately 2 mL/min. Once the pumping began, a third pump was used to pump the titanium solution directly into the transition-metal solution at 2 mL/min. The temperature and nitrogen protection were maintained throughout the reaction, and the base pumping was tuned to maintain a pH of 10.5 ± 0.1. The stirring rate was gradually increased to maintain a consistent vortex in solution as volume increased. The precipitate was collected using vacuum filtration and washed with 400 mL of DI water and then 400 mL of isopropanol. The precipitate was dried in a vacuum oven overnight at 100 °C. The precursor and LiOH were mixed thoroughly and calcined under pure oxygen flow at 0.5 L/min. The calcination procedure involved heating at 5 °C/min to 460 °C and holding for 1 h, and then heating at 5 °C/min to 725 °C and holding for 6 h. Finally, it was cooled at 5 °C/min to 25 °C under constant oxygen flow to obtain the final powder (i.e., "gradient substitution"). The "bulk substitution" samples were synthesized by having the titanium oxysulfate directly in the transition-metal solution. The "surface substitution" samples were synthesized by precipitating $Ti(OH)_4$ after the (Ni, Mn, Co) hydroxide precipitation was completed. The baseline NMC811 was synthesized following a similar procedure but without the titanium oxysulfate. The electrode preparation and battery testing method remained similar to our previous work and is referenced here.[7] The methods for XRD, STEM-EELS, soft XAS, and hard XAS were provided in our earlier publications and are referenced here.[5,7,40,41]

**Theoretical Calculation Method.** The time-dependent density functional theory (TDDFT) based X-ray absorption near-edge structure (XANES) calculations, as implemented in Finite Difference Method Near Edge Structure (FDMNES) package,[42] have been performed for Ti-substituted $Li_{1-x}TMO_2$. Within the TDDFT method, the partly localized edges ($L_{23}$-edges of transition-metal Ti) can be described quite correctly beyond the most common density functional theory (DFT).

First, to provide the quantitative experimental quantity for theoretical modeling, we perform the peak fitting for the experimental XAS spectra of Ti L-edge with different lithium concentrations. In such a way, we are able to set up an experimental database of FWHM, area, and position of Ti L-edge peaks. Typical fitting results are shown in Figure S4 for example. One can clearly see the trend of broadening character of Ti L-edge during the delithiation process. Second, the XANES calculation of Ti-substituted $Li_{1-x}TMO_2$ has been done with TDDFT-based Finite Difference Method using a cluster model. The XANES calculations were performed on clusters containing 66 atoms and with the convolution widths of 1.2 eV for $L_2$- and $L_3$-edge, respectively. A theoretical database of XANES as a function of Ti−O bond length and lithium concentration has been thus obtained. Figure S5a,b shows typical XANES results for two different Li concentrations as a function of Ti−O bond length.

Third, first-principles total energy calculations based on DFT has been done for Ti-substituted $Li_{1-x}TMO_2$ to obtain the trend of Ti−O bond length changed with Ti substituting and Li concentration. The Vegard's law of lattice change is thus verified with changes of Li concentration.

Finally, the theoretical model of XANES as a function of Ti−O bond length and lithium concentration has been built and fitted to experimental data, utilizing the obtained trends of XANES vs bond length (Figure S5a,b) and the Vegard's law for lattice changed with lithium concentrations $x$. The fitting formula of $Li_{1-x}TMO_2$ can be expressed as

$$\text{FWHM} = (w_{00} + w_{01}x) - (w_{10} + w_{11}x)b(x)$$

$$\text{area} = (\alpha_{00} + \alpha_{01}x) - (\alpha_{10} + \alpha_{11}x)b(x)$$

where $b(x) = b_0 - b_1x$ is the bong length of Ti−O and $b_0$ and $b_1$ are coefficient parameters. The best fitted parameters are listed below: $w_{00}$ = 6.80, $w_{01}$ = 11.05, $w_{10}$ = 2.79, $w_{11}$ = 5.65; $\alpha_{00}$ = 7.00, $\alpha_{01}$ = −1.86, $\alpha_{10}$ = 2.73, $\alpha_{11}$ = −0.86; $b_0$ = 2.06, $b_1$ = 0.12. The comparison of fitting results from theoretical model and experiments are shown in Figure S5c,d.

## ■ ASSOCIATED CONTENT

### Supporting Information

The Supporting Information is available free of charge on the ACS Publications website at DOI: 10.1021/acsami.9b14729.

Experimental methods, DFT calculation, synchrotron X-ray results, and batteries performance (PDF)

## ■ AUTHOR INFORMATION


### Corresponding Author

*E-mail: fenglin@vt.edu. Phone: (540) 231-4067.

### ORCID

Linqin Mu: 0000-0003-4421-4820

Muhammad Mominur Rahman: 0000-0001-6814-456X

Wei Luo: 0000-0002-4019-4634

Feng Lin: 0000-0002-3729-3148


### Author Contributions

F.L. supervised the project. J.D.S., J.W, and B.Z. performed synthesis, performance testing, and characterization. Y.Z., L.M., Z.X., M.M.R, C.-J. S., and D.N. performed X-ray spectroscopy.



DOI: 10.1021/acsami.9b14729
ACS Appl. Mater. Interfaces 2019, 11, 37885−37891

F.M.M. performed XRD. H.C. and J.C.Z performed the DFT calculation. H.L.X. performed STEM-EELS. H.S. and W.L. participated in the data interpretation. F.L. and J.D.S. analyzed the data and wrote the manuscript.

### Notes

The authors declare no competing financial interest.

## ■ ACKNOWLEDGMENTS

This material is based upon work supported by the U.S. Department of Energy's Office of Energy Efficiency and Renewable Energy (EERE) under the Award Number: DE-EE0008444. Use of the Stanford Synchrotron Radiation Lightsource, SLAC National Accelerator Laboratory, is supported by the U.S. Department of Energy, Office of Science, Office of Basic Energy Sciences under Contract No. DE-AC02-76SF00515. This research used resources of the Center for Functional Nanomaterials, Brookhaven National Laboratory, which is supported by the U.S. Department of Energy, Office of Basic Energy Sciences under Contract No. DE-SC0012704. This research used resources of the Advanced Photon Source, a U.S. Department of Energy (DOE) Office of Science User Facility operated for the DOE Office of Science by Argonne National Laboratory under Contract No. DE-AC02-06CH11357. H.C. and J.-C.Z. acknowledge Special Program for Applied Research on Super Computation of the NSFC-Guangdong Joint Fund (the second phase) under Grant No. U1501501. This report was prepared as an account of work sponsored by an agency of the United States Government. Neither the United States Government nor any agency thereof, nor any of their employees, makes any warranty, express or implied, or assumes any legal liability or responsibility for the accuracy, completeness, or usefulness of any information, apparatus, product, or process disclosed, or represents that its use would not infringe privately owned rights. Reference herein to any specific commercial product, process, or service by trade name, trademark, manufacturer, or otherwise does not necessarily constitute or imply its endorsement, recommendation, or favoring by the United States Government or any agency thereof. The views and opinions of authors expressed herein do not necessarily state or reflect those of the United States Government or any agency thereof.

## ■ REFERENCES

(1) Dunn, B.; Kamath, H.; Tarascon, J.-M. Electrical Energy Storage for the Grid: A Battery of Choices. *Science* **2011**, *334* (6058), 928–935.

(2) Van Noorden, R. The Rechargeable Revolution: A Better Battery. *Nature* **2014**, *507*, 26–28.

(3) Goodenough, J. B.; Kim, Y. Challenges for Rechargeable Li Batteries. *Chem. Mater.* **2010**, *22* (3), 587–603.

(4) Whittingham, M. S. Lithium Batteries and Cathode Materials. *Chem. Rev.* **2004**, *104* (10), 4271–4302.

(5) Lin, F.; Nordlund, D.; Markus, I. M.; Weng, T.-C.; Xin, H. L.; Doeff, M. M. Profiling the Nanoscale Gradient in Stoichiometric Layered Cathode Particles for Lithium-Ion Batteries. *Energy Environ. Sci.* **2014**, *7*, 3077–3085.

(6) Li, W.; Dolocan, A.; Oh, P.; Celio, H.; Park, S.; Cho, J.; Manthiram, A. Dynamic Behaviour of Interphases and Its Implication on High-Energy-Density Cathode Materials in Lithium-Ion Batteries. *Nat. Commun.* **2017**, *8*, 14589.

(7) Steiner, J. D.; Mu, L.; Walsh, J.; Rahman, M. M.; Zydlewski, B.; Michel, F. M.; Xin, H. L.; Nordlund, D.; Lin, F. Accelerated Evolution of Surface Chemistry Determined by Temperature and Cycling History in Nickel-Rich Layered Cathode Materials. *ACS Appl. Mater. Interfaces* **2018**, *10* (28), 23842–23850.

(8) Lin, F.; Markus, I. M.; Nordlund, D.; Weng, T.-C.; Asta, M. D.; Xin, H. L.; Doeff, M. M. Surface Reconstruction and Chemical Evolution of Stoichiometric Layered Cathode Materials for Lithium-Ion Batteries. *Nat. Commun.* **2014**, *5* (1), 3529.

(9) Jung, R.; Metzger, M.; Maglia, F.; Stinner, C.; Gasteiger, H. A. Oxygen Release and Its Effect on the Cycling Stability of LiNi x Mn y Co z O 2 (NMC) Cathode Materials for Li-Ion Batteries. *J. Electrochem. Soc.* **2017**, *164* (7), A1361–A1377.

(10) Huang, Q.; Ma, L.; Liu, A.; Ma, X.; Li, J.; Wang, J.; Dahn, J. R. The Reactivity of Charged Positive $Li_{1-n}[Ni_xMn_yCo_z]O_2$ Electrodes with Electrolyte at Elevated Temperatures Using Accelerating Rate Calorimetry. *J. Power Sources* **2018**, *390*, 78–86.

(11) Myung, S. T.; Maglia, F.; Park, K. J.; Yoon, C. S.; Lamp, P.; Kim, S. J.; Sun, Y. K. Nickel-Rich Layered Cathode Materials for Automotive Lithium-Ion Batteries: Achievements and Perspectives. *ACS Energy Letters* **2017**, *2*, 196–223.

(12) Zheng, J.; Kan, W. H.; Manthiram, A. Role of Mn Content on the Electrochemical Properties of Nickel-Rich Layered $LiNi_{0.8-x}Co_{0.1}Mn_{0.1+x}O_2$ ($0.0 < x < 0.08$) Cathodes for Lithium-Ion Batteries. *ACS Appl. Mater. Interfaces* **2015**, *7* (12), 6926–6934.

(13) Liu, W.; Oh, P.; Liu, X.; Lee, M.-J.; Cho, W.; Chae, S.; Kim, Y.; Cho, J. Nickel-Rich Layered Lithium Transition-Metal Oxide for High-Energy Lithium-Ion Batteries. *Angew. Chem., Int. Ed.* **2015**, *54* (15), 4440–4457.

(14) Zheng, J.; Liu, T.; Hu, Z.; Wei, Y.; Song, X.; Ren, Y.; Wang, W.; Rao, M.; Lin, Y.; Chen, Z.; Lu, J.; Wang, C.; Amine, K.; Pan, F. Tuning of Thermal Stability in Layered $Li(Ni_xMn_yCo_z)O_2$. *J. Am. Chem. Soc.* **2016**, *138* (40), 13326–13334.

(15) Wu, F.; Tian, J.; Liu, N.; Lu, Y.; Su, Y.; Wang, J.; Chen, R.; Ma, X.; Bao, L.; Chen, S. Alleviating Structural Degradation of Nickel-Rich Cathode Material by Eliminating the Surface $Fm\bar{3}m$ Phase. *Energy Storage Mater.* **2017**, *8*, 134–140.

(16) Mao, C.; Wood, M.; David, L.; An, S. J.; Sheng, Y.; Du, Z.; Meyer, H. M.; Ruther, R. E.; Wood, D. L. Selecting the Best Graphite for Long-Life, High-Energy Li-Ion Batteries. *J. Electrochem. Soc.* **2018**, *165* (9), A1837–A1845.

(17) Dixit, M.; Markovsky, B.; Schipper, F.; Aurbach, D.; Major, D. T. Origin of Structural Degradation during Cycling and Low Thermal Stability of Ni-Rich Layered Transition Metal-Based Electrode Materials. *J. Phys. Chem. C* **2017**, *121* (41), 22628–22636.

(18) Mu, L.; Lin, R.; Xu, R.; Han, L.; Xia, S.; Sokaras, D.; Steiner, J. D.; Weng, T.-C.; Nordlund, D.; Doeff, M. M.; Liu, Y.; Zhao, K.; Xin, H. L.; Lin, F. Oxygen Release Induced Chemomechanical Breakdown of Layered Cathode Materials. *Nano Lett.* **2018**, *18* (5), 3241–3249.

(19) Tian, C.; Xu, Y.; Nordlund, D.; Lin, F.; Liu, J.; Sun, Z.; Liu, Y.; Doeff, M. Charge Heterogeneity and Surface Chemistry in Polycrystalline Cathode Materials. *Joule* **2018**, *2* (3), 464–477.

(20) Jung, S.-K.; Gwon, H.; Hong, J.; Park, K.-Y.; Seo, D.-H.; Kim, H.; Hyun, J.; Yang, W.; Kang, K. Understanding the Degradation Mechanisms of $LiNi_{0.5}Co_{0.2}Mn_{0.3}O_2$ Cathode Material in Lithium Ion. *Batteries. Adv. Energy Mater.* **2014**, *4*, 1300787.

(21) Jung, R.; Metzger, M.; Maglia, F.; Stinner, C.; Gasteiger, H. A. Oxygen Release and Its Effect on the Cycling Stability of $LiNi_xMn_yCo_zO_2$ (NMC) Cathode Materials for Li-Ion Batteries. *J. Electrochem. Soc.* **2017**, *164* (7), A1361–A1377.

(22) Xiao, B.; Liu, H.; Liu, J.; Sun, Q.; Wang, B.; Kaliyappan, K.; Zhao, Y.; Banis, M. N.; Liu, Y.; Li, R.; Sham, T.-K.; Botton, G. A.; Cai, M.; Sun, X. Nanoscale Manipulation of Spinel Lithium Nickel Manganese Oxide Surface by Multisite Ti Occupation as High-Performance Cathode. *Adv. Mater.* **2017**, *29* (47), 1703764.

(23) Markus, I. M.; Lin, F.; Kam, K. C.; Asta, M.; Doeff, M. M. Computational and Experimental Investigation of Ti Substitution in $Li1(Ni_xMn_xCo_{1-2x-y}Ti_y)O_2$ for Lithium-Ion Batteries. *J. Phys. Chem. Lett.* **2014**, *5* (21), 3649–3655.

(24) Sun, H.; Cao, Z.; Wang, T.; Lin, R.; Li, Y.; Liu, X.; Zhang, L.; Lin, F.; Huang, Y.; Luo, W. Enabling High Rate Performance of Ni-



DOI: 10.1021/acsami.9b14729
*ACS Appl. Mater. Interfaces* 2019, 11, 37885–37891

Rich Layered Oxide Cathode by Uniform Titanium Doping. *Mater. Today Energy* **2019**, *13*, 145−151.
(25) Wise, A. M.; Ban, C.; Weker, J. N.; Misra, S.; Cavanagh, A. S.; Wu, Z.; Li, Z.; Whittingham, M. S.; Xu, K.; George, S. M.; Toney, M. F. Effect of $Al_2O_3$ Coating on Stabilizing $LiNi_{0.4}Mn_{0.4}Co_{0.2}O_2$ Cathodes. *Chem. Mater.* **2015**, *27* (17), 6146−6154.
(26) Mohanty, D.; Dahlberg, K.; King, D. M.; David, L. A.; Sefat, A. S.; Wood, D. L.; Daniel, C.; Dhar, S.; Mahajan, V.; Lee, M.; Albano, F. Modification of Ni-Rich FCG NMC and NCA Cathodes by Atomic Layer Deposition: Preventing Surface Phase Transitions for High-Voltage Lithium-Ion Batteries. *Sci. Rep.* **2016**, *6* (1), 26532.
(27) Laskar, M. R.; Jackson, D. H. K.; Guan, Y.; Xu, S.; Fang, S.; Dreibelbis, M.; Mahanthappa, M. K.; Morgan, D.; Hamers, R. J.; Kuech, T. F. Atomic Layer Deposition of $Al_2O_3 - Ga_2O_3$ Alloy Coatings for $Li[Ni_{0.5}Mn_{0.3}Co_{0.2}]O_2$ Cathode to Improve Rate Performance in Li-Ion Battery. *ACS Appl. Mater. Interfaces* **2016**, *8* (16), 10572−10580.
(28) Dogan, F.; Vaughey, J. T.; Iddir, H.; Key, B. Direct Observation of Lattice Aluminum Environments in Li Ion Cathodes $LiNi_{1-y-z}Co_yAl_zO_2$ and Al-Doped $LiNi_xMn_yCo_zO_2$ via $^{27}Al$ MAS NMR Spectroscopy. *ACS Appl. Mater. Interfaces* **2016**, *8* (26), 16708−16717.
(29) Riley, L. A.; Van Atta, S.; Cavanagh, A. S.; Yan, Y.; George, S. M.; Liu, P.; Dillon, A. C.; Lee, S.-H. Electrochemical Effects of ALD Surface Modification on Combustion Synthesized $LiNi_{1/3}Mn_{1/3}Co_{1/3}O_2$ as a Layered-Cathode Material. *J. Power Sources* **2011**, *196* (6), 3317−3324.
(30) Patoux, S.; Doeff, M. M. Direct Synthesis of $LiNi_{1/3}Co_{1/3}Mn_{1/3}O_2$ from Nitrate Precursors. *Electrochem. Commun.* **2004**, *6* (3), 767−772.
(31) Lin, F.; Markus, I. M.; Nordlund, D.; Weng, T.-C.; Asta, M. D.; Xin, H. L.; Doeff, M. M. Surface Reconstruction and Chemical Evolution of Stoichiometric Layered Cathode Materials for Lithium-Ion Batteries. *Nat. Commun.* **2014**, *5*, 3529.
(32) Mu, L.; Rahman, M. M.; Zhang, Y.; Feng, X.; Du, X.-W.; Nordlund, D.; Lin, F. Surface Transformation by a "Cocktail" Solvent Enables Stable Cathode Materials for Sodium Ion Batteries. *J. Mater. Chem. A* **2018**, *6* (6), 2758−2766.
(33) Zhang, J.-N.; Li, Q.; Ouyang, C.; Yu, X.; Ge, M.; Huang, X.; Hu, E.; Ma, C.; Li, S.; Xiao, R.; Yang, W.; Chu, Y.; Liu, Y.; Yu, H.; Yang, X.-Q.; Huang, X.; Chen, L.; Li, H. Trace Doping of Multiple Elements Enables Stable Battery Cycling of $LiCoO_2$ at 4.6 V. *Nat. Energy* **2019**, *4* (7), 594−603.
(34) Zhao, E.; Chen, M.; Hu, Z.; Chen, D.; Yang, L.; Xiao, X. Improved Cycle Stability of High-Capacity Ni-Rich $LiNi_{0.8}Mn_{0.1}Co_{0.1}O_2$ at High Cut-off Voltage by $Li_2SiO_3$ Coating. *J. Power Sources* **2017**, *343*, 345−353.
(35) Li, J.; Downie, L. E.; Ma, L.; Qiu, W.; Dahn, J. R. Study of the Failure Mechanisms of $LiNi_{0.8}Mn_{0.1}Co_{0.1}O_2$ Cathode Material for Lithium Ion Batteries. *J. Electrochem. Soc.* **2015**, *162* (7), A1401−A1408.
(36) Xie, J.; Sendek, A. D.; Cubuk, E. D.; Zhang, X.; Lu, Z.; Gong, Y.; Wu, T.; Shi, F.; Liu, W.; Reed, E. J.; Cui, Y. Atomic Layer Deposition of Stable $LiAlF_4$ Lithium Ion Conductive Interfacial Layer for Stable Cathode Cycling. *ACS Nano* **2017**, *11* (7), 7019−7027.
(37) Zhao, W.; Zheng, J.; Zou, L.; Jia, H.; Liu, B.; Wang, H.; Engelhard, M. H.; Wang, C.; Xu, W.; Yang, Y.; Zhang, J.-G. High Voltage Operation of Ni-Rich NMC Cathodes Enabled by Stable Electrode/Electrolyte Interphases. *Adv. Energy Mater.* **2018**, *8* (19), 1800297.
(38) Yan, P.; Zheng, J.; Liu, J.; Wang, B.; Cheng, X.; Zhang, Y.; Sun, X.; Wang, C.; Zhang, J.-G. Tailoring Grain Boundary Structures and Chemistry of Ni-Rich Layered Cathodes for Enhanced Cycle Stability of Lithium-Ion Batteries. *Nat. Energy* **2018**, *3* (7), 600−605.
(39) Wolff-Goodrich, S.; Lin, F.; Markus, I. M.; Nordlund, D.; Xin, H. L.; Asta, M.; Doeff, M. M. Tailoring the Surface Properties of $LiNi_{0.4}Mn_{0.4}Co_{0.2}O_2$ by Titanium Substitution for Improved High Voltage Cycling Performance. *Phys. Chem. Chem. Phys.* **2015**, *17* (34), 21778−21781.
(40) Mu, L.; Feng, X.; Kou, R.; Zhang, Y.; Guo, H.; Tian, C.; Sun, C.-J.; Du, X.-W.; Nordlund, D.; Xin, H. L.; Lin, F. Deciphering the Cathode-Electrolyte Interfacial Chemistry in Sodium Layered Cathode Materials. *Adv. Energy Mater.* **2018**, *8*, 1801975.
(41) Rahman, M. M.; Zhang, Y.; Xia, S.; Kan, W. H.; Avdeev, M.; Mu, L.; Sokaras, D.; Kroll, T.; Du, X.-W.; Nordlund, D.; Liu, Y.; Lin, F. Surface Characterization of Li-Substituted Compositionally Heterogeneous $NaLi_{0.045}Cu_{0.185}Fe_{0.265}Mn_{0.505}O_2$ Sodium-Ion Cathode Material. *J. Phys. Chem. C* **2019**, *123* (18), 11428−11435.
(42) Bunău, O.; Joly, Y. Self-Consistent Aspects of x-Ray Absorption Calculations. *J. Phys.: Condens. Matter* **2009**, *21* (34), 345501.


DOI: 10.1021/acsami.9b14729
*ACS Appl. Mater. Interfaces* 2019, 11, 37885−37891